Kinetics of Receptor Directed Assembly of Multisegment Nanowires

Min Chen, Lian Guo, Reena Ravi, and Peter C. Searson*

Department of Materials Science and Engineering, Johns Hopkins University, Baltimore, Maryland 21218

Received: September 14, 2005; In Final Form: October 24, 2005

We demonstrate the receptor directed end-to-end assembly of multisegment Au/Ni/Au nanowires under agitation in ethanol. The gold end-segments were functionalized with biotin-terminated thiol thereby restricting aggregation to end-to-end attachment via an avidin linkage. On mixing biotin-terminated nanowires with avidin-terminated nanowires, the average chain length is shown to increase linearly with time. The rate constant was independent of the nanowire concentration. Kinetic Monte Carlo simulations were used to model the self-assembly process, and we show that the directed end-to-end assembly of nanowires is similar to the polycondensation of linear polymers.

Introduction

The assembly of nanoscale building blocks into complex structures is an example of the bottom-up approach to device fabrication. Nonspecific chemical interactions have been exploited in the assembly of two-dimensional close packed arrays of nanoparticles[1,2] and in the assembly of face centered cubic colloidal crystals.[3−5] External electric fields have been used to create one-dimensional chains[6,7] and two-dimensional close packed arrays of nanoparticles.[8] The controlled aggregation of nanoparticles through specific biological interactions provides an alternative approach for the fabrication of novel architectures and devices.

Specific biological interactions have been exploited in the controlled aggregation of spherical gold nanoparticles[9−11] and single component gold nanorods.[12] Connolly et al.[11] and Aslan et al.[10] reported on the kinetics of controlled aggregation of biotinylated gold nanoparticles on injection of avidin. Both groups showed that, for a fixed reaction time, the aggregate size exhibited a maximum at a characteristic avidin concentration. In both cases, the aggregation of the biotinylated gold nanoparticles was analyzed in terms of Smoluchowski kinetics for aggregation.[13−15] Connolly et al.[11] concluded that the kinetics of aggregation followed a modified form of the Smoluchowski equation for diffusion-limited aggregation, taking into account the induction time required for the initial attachment of avidin to the biotinylated gold nanoparticles before aggregation can occur. Aslan et al.[10] reported that aggregation followed reaction-limited aggregation.

Multisegment nanowires or nanorods provide the opportunity for directing the assembly of more complex structures. With the wide range of metallic and semiconductor multisegment and heterojunction nanowires that have been fabricated,[16−26] there are many opportunities for the assembly of architectures with complex functions. Exploiting different ligand-surface receptor linkages allows the different segments in a multisegment nanowire to be functionalized with different terminal groups.[17,18,23,27−29] In previous work[28] we have demonstrated the directed end-to-end assembly of three segment nanowires with biotin-terminated end-segments. Directed end-to-end assembly of nanowires represents a simple model system to explore the dynamics of receptor mediated self-assembly. In this paper we reported the kinetics of end-to-end assembly of Au/Ni/Au nanowires using the avidin−biotin linkage.

Experimental Section

Electrochemical Template Synthesis of Nanowires. The building blocks in these experiments were three segment Au/Ni/Au nanowires prepared by electrochemical template synthesis. The templates were 200 nm anodized alumina membranes with a pore density of 1×10^9 cm^{-2} (Whatman, Cat. No. 6809-5022) that yielded nanowires with an average diameter of 350 nm. On the bottom of the template the pores were sealed with a 500 nm thick copper layer evaporated at 50 mA and 9×10^{-7} Torr. The template was assembled into an electrochemical cell with a platinum mesh counter electrode and a Ag/AgCl (3M NaCl) reference electrode ($U_{eq} = 0.200$ V vs SHE).

An additional 5 μm copper layer (5 C cm^{-2}) was deposited into the template at −0.2 V (Ag/AgCl) from 0.5 M $CuSO_4$ (Alfa Aesar, CAS 7758-99-8) and 0.67 M HBO_3 (Alfa Aesar, CAS 10043-35-3) (pH 3.5). The purpose of the copper layer was to fill the branched region of the alumina template prior to nanowire deposition. A 10 nm gold layer (0.0625 C cm^{-2}) was deposited at −1.0 V from a commercial gold plating solution (Technic Inc., Cat. No. F2-5-1742), followed by a 4 μm nickel layer (10 C cm^{-2}) deposited at −1.0 V from 0.5 M $NiSO_4$ (Sigma-Aldrich, CAS 10101-97-0), 0.67 M HBO_3 (Alfa Aesar, CAS 10043-35-3) (pH 3.5), and finally a second 10 nm gold layer was deposited using the same conditions as reported above.

After deposition, the evaporated copper layer on the backside of the template and the electrodeposited copper ends of the nanowires were dissolved in 0.3 M $CuCl_2$ and 0.5 M HCl. The alumina templates were then dissolved in 2 M NaOH (J. T. Baker, CAS 1310-73-2) at 40 °C overnight. After the template was dissolved, the nanowires were washed with deionized water and absolute ethanol (Pharmco, ACS grade) several times. The nanowires were then collected by centrifugation at 1500 rpm for 20 min. After fresh solvent was added, the nanowires were then resuspended by sonicatation for 10 min. Nanowire concentrations in suspension were estimated from the area of the template used for deposition and the pore density.

Synthesis of Biotin-terminated Thiol. 11-(15-(Biotinoylamino)-4,7,10,13-tetraoxapentanoylamino)undecanethiol (BTT)

* To whom correspondence should be addressed. E-mail: searson@jhu.edu.

10.1021/jp055204m CCC: $33.50
Published on Web 12/15/2005

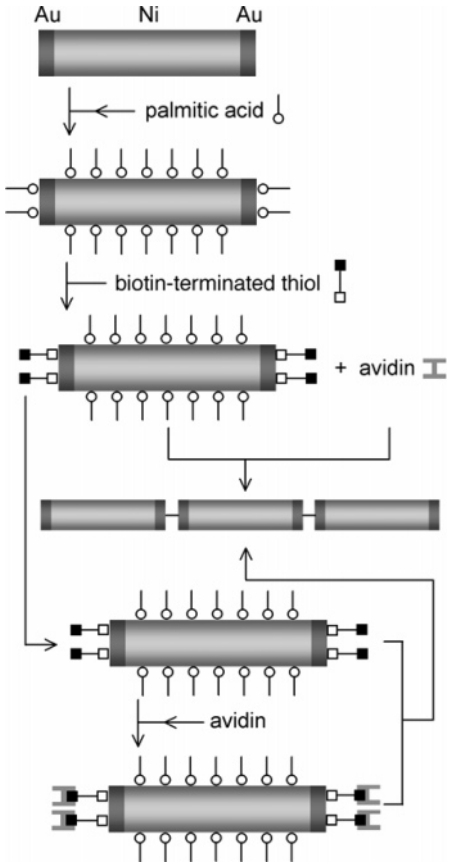

Figure 1. Schematic illustration of the functionalization and self-assembly of Au/Ni/Au nanowires. The central nickel segments are functionalized with palmitic acid. The gold end-segments are functionalized with biotin-terminated thiol. Self-assembly experiments were performed either by mixing biotin-terminated nanowires with avidin or by mixing biotin-terminated nanowires with avidin-terminated nanowires.

was synthesized as reported elsewhere.[28] Briefly, 2.4 mg 11-amino-1-undecanethiol (Dojindo, Cat. No. A423-10, CAS 143339-58-6) was reacted with 5.89 mg *N*-hydroxy-succinimide-tetraethylene glycol-biotin (Pierce, Cat. No. 21330) in 5 mL of a 50:50 mixture of dimethylformamide (Aldrich, CAS 68-12-2) and dimethyl sulfoxide (Aldrich, CAS 67-68-5) overnight under an argon blanket at room temperature. All reagents were used as-received and no further purification was performed. After synthesis, the BTT was diluted into a 5 mM ethanol solution. The biotin is attached to the gold end-segments of the nanowires through the thiol group, forming a self-assembled monolayer on the gold surface.

Surface Functionalization of Nanowires. The selective functionalization of Au/Ni/Au nanowires is illustrated schematically in Figure 1. The Au/Ni/Au nanowires were exposed to palmitic acid ($CH_3(CH_2)_{14}COOH$, Aldrich, CAS 57-10-3) and biotinylated thiol in ethanol solution. In a 1 mL plastic vial, 100 μL of a nanowire suspension (1.25×10^9 cm^{-3}) was mixed with 100 μL of palmitic acid (5 mM) and 20 μL of biotinylated thiol (5 mM) in ethanol. The vial was placed on a shaker for 6 h. The excess biotinylated thiol and palmitic acid were then removed by centrifugation and rinsing with pure ethanol several times.

Avidin-terminated nanowires were prepared in the following way. First, 10 μL of a suspension of biotin-terminated nanowires was injected into 1 mL of a 76 nM (5 μg mL^{-1}) solution of avidin (Invitrogen, Cat. No. A-2667) in ethanol to give a nanowire concentration of 2.1×10^{-17} M (1.25×10^7 cm^{-3}).

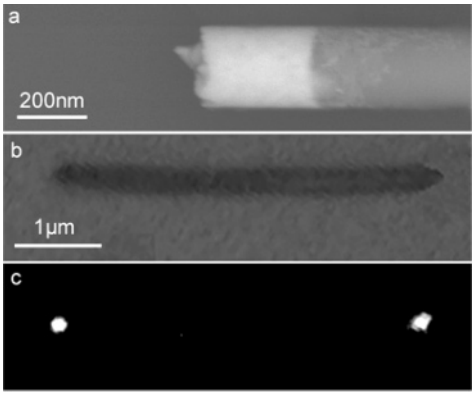

Figure 2. (a) SEM image of a Au/Ni/Au nanowire. (b) Optical microscope image of a Au/Ni/Au nanowire with a 4 μm nickel segments and 300 nm gold segments. The gold end-segments of the nanowire have been functionalized with NATR. (c) Corresponding fluorescence image showing that avidin is bound to the Au end-segments. Note that all of the self-assembly experiments were performed with 10 nm Au end-segments to maximize the probability of end-to-end attachment.

For fluorescence experiments, the nanowires were functionalized with NeutraAvidin tetramethyl rhodamine (NATR, Invitrogen, Cat. No. A-6373). After the reaction was shaken for 1 h, excess avidin was removed by centrifugation and rinsing with pure ethanol several times. In previous work, we have shown that in ethanol nonspecific binding of avidin to nanowires with nonbiotinylated segments can be minimized, resulting in effective differential functionalization for self-assembly and tethering.[28,29]

Self-Assembly of Nanowires. Self-assembly experiments were performed in two ways, as shown schematically in Figure 1. Experiments involving the directed assembly of biotin-terminated nanowires and avidin-terminated nanowires require that we first determine conditions for producing avidin-terminated nanowires with minimum end-to-end binding. Thus, in the first series of experiments we report on the addition of avidin to biotin-terminated nanowires. In these experiments, 100 μL of a suspension of nanowires with biotin-terminated gold end-segments was injected into 1 mL of 8−200 nM avidin in ethanol in a 1.5 mL vial to give a nanowire concentration of 2.1×10^{-16} M (1.25×10^8 cm^{-7}). The vial was then placed on a shaker for up to 6 h.

In the second series of experiments, nanowires with biotin-terminated gold end-segments were mixed with the same number of nanowires with avidin-terminated gold end-segments in a vial on a shaker. The total concentration of nanowires (avidin-terminated and biotin-terminated) was in the range 5×10^6 to 1.25×10^8 cm^{-3}.

The time dependence of the chain length distribution was obtained by extracting small aliquots of the suspension (~1 μL) and injecting into a large volume (1 mL) of ethanol to effectively stop the assembly reaction. Finally, drops of the diluted nanowire suspension were placed on glass slides and observed on an optical microscope. The nanowire chain length distributions were obtained by counting 200−1000 nanowire chains.

Results and Discussion

Self-Assembly of Au/Ni/Au Nanowires. Figure 2 shows optical and fluorescence microscope images of a Au/Ni/Au nanowire where the biotinylated thiol is conjugated with fluorescently labeled avidin (NATR). For convenience these nanowires were fabricated with 300 nm gold end-segments. The

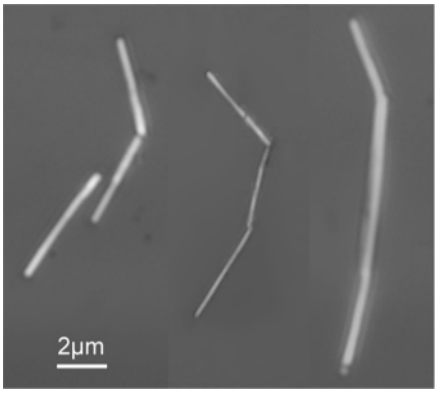

Figure 3. Optical images of a single unattached Au/Ni/Au nanowire and nanowire chains with two, three, and four nanowires.

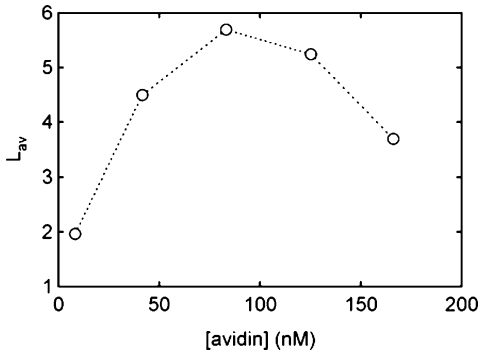

Figure 4. Average chain length vs avidin concentration for experiments where nanowires with biotin-terminated gold end-segments were injected into ethanol with different avidin concentrations. The nanowire concentration was 2.1×10^{-16} M (1.25×10^8 cm^{-3}), and the reaction time was 3 min.

fluorescence image confirms that nonspecific binding of avidin to the central nickel segments is prevented by selective binding of palmitic acid to the native oxide on the nickel segment. Figure 2a shows the corresponding SEM image of a nanowire showing the gold end-segment.

Figure 3 shows typical optical microscope images obtained from assembly experiments with Au(10 nm)/Ni(4 μm)/Au(10 nm) nanowires. The 10 nm Au end-segments maximize the probability of end-to-end attachment and minimize overlap and nodes with more than two nanowires.

Figure 4 shows the average nanowire chain length (L_{av}) vs the avidin concentration for a nanowire concentration of 1.25×10^7 cm^{-3} and a reaction time of 3 min. The average chain length exhibits a maximum at an avidin concentration of 83 nM corresponding to 4.0×10^8 avidin molecules per nanowire. Similar results have been reported for the receptor-mediated aggregation of biotin-terminated gold nanoparticles in aqueous solution.[10,11] The peak corresponds to a relatively large avidin concentration, however, our experiments were performed in ethanol where the specific activity is expected to be significantly lower[30] than in water where the specific activity of 13.5 U mg^{-1} corresponds to about 3.7 biotin groups per avidin.

The assembly of biotin-terminated nanowires in suspension with avidin involves two steps: (i) the reaction of avidin with nanowire end-segments that have unoccupied biotin sites and (ii) the reaction of a biotin-terminated end segment with an avidin-terminated end segment. Since free avidin molecules have much higher mobility than the avidin-terminated nanowires, the first step is expected to be significantly faster than the second. Note that in the first step there is no assembly of nanowires (no increase in chain length) and no consumption of single nanowires. Only the second step involves the assembly of two nanowires and the consumption of single nanowires. Thus, the rate of assembly is determined by the second step and can be determined by examining time dependence of the fraction of single nanowires.

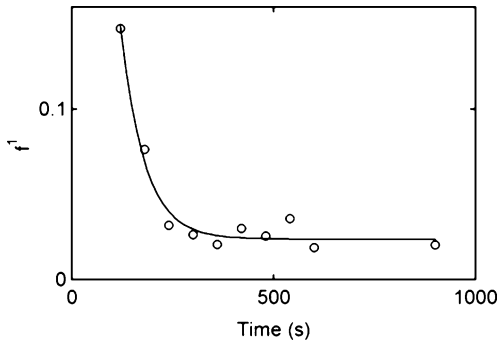

Figure 5. Fraction of single nanowires vs time for experiments where Au/Ni/Au nanowires with biotin-terminated end-segments were injected into a 200 nM solution of avidin in ethanol. Experiments were performed on a shaker, and small aliquots extracted from the suspension at different times. The nanowire concentration was 2.1×10^{-16} M (1.25×10^8 cm^{-7}). The solid line corresponds to a fit to eq 1.

Figure 5 shows the fraction of single nanowires vs reaction time. In this experiment, 1.25×10^8 Au/Ni/Au nanowires with biotin-terminated end-segments were injected into a 200 nM solution of avidin in ethanol. The fraction of single nanowires (f^1) was obtained based on counting all single nanowires and nanowire chains.

With excess avidin, we can assume that the concentration of avidin-terminated nanowires is much larger than the concentration of biotin-terminated nanowires and hence the second step becomes pseudo first order in the concentration of biotin-terminated nanowires and we can write

$$f^1 = n/n_0 = \exp(-kt) \tag{1}$$

The solid line in Figure 5 is an exponential fit of the form: $f^1 = 0.024 + 0.96 \exp(-t/58.7)$ from which we obtain $k = 0.017 \pm 0.003$ s^{-1} and $t_{1/2} = 40.8$ s.

Directed End-to-End Assembly of Biotin-Terminated Nanowires and Avidin-Terminated Nanowires. In the second series of experiments, biotin-terminated nanowires (B−B) were mixed with an equal number of avidin-terminated nanowires (A−A). The reaction can be written as

$$\text{A}-\text{A} + \text{B}-\text{B} \rightarrow \text{A}-\text{AB}-\text{B} \tag{2}$$

Figure 6 shows the distributions of nanowire chains obtained for an initial nanowire concentration $n_{A-A} = n_{B-B} = 2.5 \times 10^7$ cm^{-3} after 10, 30, 50, and 60 min. n_{A-A} and n_{B-B} represent the number density of avidin-terminated nanowires and biotin-terminated nanowires, respectively. The total number of single nanowires in the solution at the start of the experiment $n_0 = 2n_{A-A} = 2n_{B-B}$. From Figure 6, it can be seen that the average chain length and the width of the distribution both increase with time.

From the distributions we can determine the time dependence of the average chain length and the fraction of single (unattached) nanowires. The average chain length L_{av} is given by

$$L_{av} = \sum_l l n^l \tag{3}$$

where n^l is the density of chains of length l.

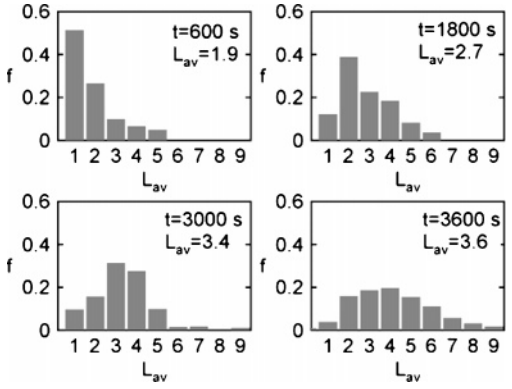

Figure 6. Histograms of nanowire chain length distribution at different times for an initial nanowire concentration $n_0 = 5 \times 10^6$ cm^{-3}. Experiments were performed by adding nanowires with biotin-terminated end-segments to nanowires with avidin-terminated end-segments

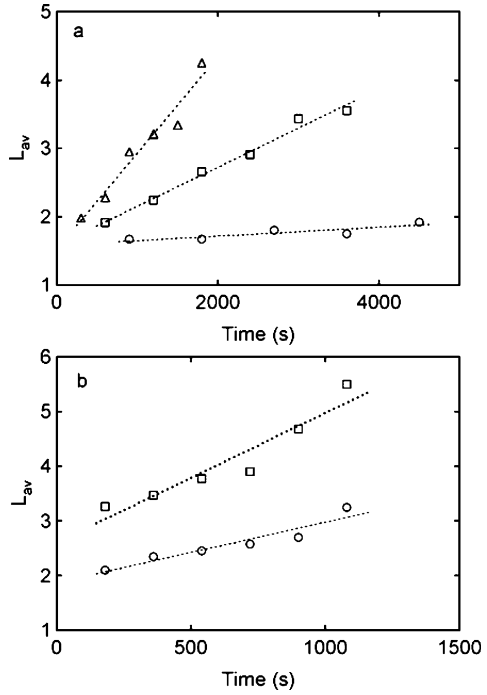

Figure 7. (a) Average chain size vs time for three experiments with initial nanowire concentrations $n_0 = (\bigcirc)\ 5 \times 10^6$ cm^{-3}, $(\square)\ 5 \times 10^7$ cm^{-3}, and $(\triangle)\ 1.25 \times 10^8$ cm^{-3}. (b) Average chain size vs time for two experiments with initial nanowire concentrations of $n_0 = (\bigcirc)\ 1.25 \times 10^7$ cm^{-3} and $(\square)\ 2.5 \times 10^7$ cm^{-3}.

Figure 7a shows a plot of the average chain length L_{av} vs time for three experiments with total nanowire concentrations (n_0) varied from 5×10^6 cm^{-3} to 1.25×10^8 cm^{-3}. Figure 7b shows a plot of average chain length L_{av} vs time for two experiments with total nanowire concentrations (n_0) of 1.25×10^7 cm^{-3} and 2.5×10^7 cm^{-3}. The experiments in Figure 7b were performed at a much larger shaking rate which results in faster assembly.

Kinetics of Directed End-to-End Assembly. To explain the kinetics of self-assembly, we have performed kinetic Monte Carlo simulations. In determining the kinetics of self-assembly we recognize that there are three types of nanowires and nanowire chains in the suspension, as illustrated in Figure 8. Chains with an odd number of nanowires have either two avidin-terminated end-segments (type α) or two biotin-terminated end-segments (type β). Conversely, chains with an even number of nanowires have one biotin-terminated end-segment and one

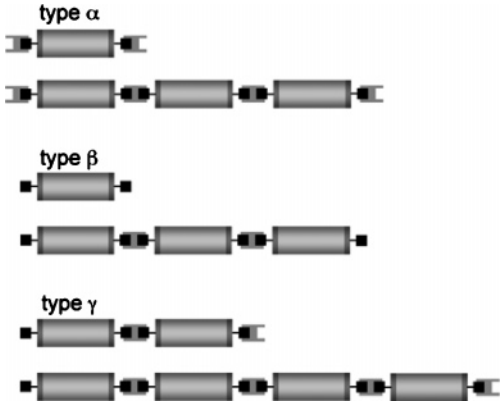

Figure 8. Nanowire chains. In the self-assembly of nanowires with biotin-terminated end-segments (B−B) and avidin-terminated end-segments (A−A) there are three types of nanowire chains: type α chains (or nanowires) with two avidin-terminated end-segments, type β chains (or nanowires) with two biotin-terminated end-segments, and type γ chains with one avidin-terminated end-segment and one biotin-terminated end-segment.

avidin-terminated end-segment (type γ). From these chains we can consider four possible attachment events. First, the attachment of a type α chain (or nanowire) with a type β chain (or nanowire) will result in the formation of a type γ chain (i.e., $\alpha + \beta \rightarrow \gamma$). Similarly we can write $\alpha + \gamma \rightarrow \alpha$, $\beta + \gamma \rightarrow \beta$, and $\gamma + \gamma \rightarrow \gamma$.

We can write rate expressions for the change in density of chains of type i (α, β, γ) resulting from the four possible attachment events:

$$\alpha + \beta \rightarrow \gamma \quad \frac{dn_{\gamma(\alpha+\beta)}^{l_1+l_2}}{dt} = k_{\alpha\beta} n_\alpha^{l_1} n_\beta^{l_2} \tag{4}$$

$$\alpha + \gamma \rightarrow \alpha \quad \frac{dn_{\alpha(\alpha+\gamma)}^{l_1+l_2}}{dt} = k_{\alpha\gamma} n_\alpha^{l_1} n_\gamma^{l_2} \tag{5}$$

$$\beta + \gamma \rightarrow \beta \quad \frac{dn_{\beta(\beta+\gamma)}^{l_1+l_2}}{dt} = k_{\beta\gamma} n_\beta^{l_1} n_\gamma^{l_2} \tag{6}$$

$$\gamma + \gamma \rightarrow \gamma \quad \frac{dn_{\gamma(\gamma+\gamma)}^{l_1+l_2}}{dt} = k_{\gamma\gamma} n_\gamma^{l_1} n_\gamma^{l_2} \tag{7}$$

where dn represents the increase in density of chains of type i resulting from an attachment event, n_i^l is the number density of chains of type i and length l, and the k's are the rate constants (units cm^3 s^{-1}) for the four different attachment reactions. Consideration of the possible configurations for each attachment event shows that the rate constants are related by $k_{\alpha\beta} = 2k_{\alpha\gamma} = 2k_{\beta\gamma} = 2k_{\gamma\gamma}$. The rate constants represent the rates of end-to-end collisions and are analogous to the rate constant in irreversible diffusion-limited aggregation theory.[31] For convenience, we define $k_{\alpha\beta} = k$.

In the simulations we define N_i^l as the number of nanowire chains of type i and length l. We start with the same number of type α and type β nanowires; at time $t = 0$, $N_0 = 2N_\alpha{}^1 = 2N_\beta{}^1$. In each time step two chains are randomly selected from the overall population and an attachment event proceeds with a probability that is determined by the corresponding rate constant. The time increment is proportional to the reciprocal of the rate constants summed over all possible reactions in the system. For example, starting with single type α and type β nanowires, the first attachment event involves the formation of a type γ chain

of length 2. After one attachment event the elapsed time is given by

$$\Delta t\langle\{n_\alpha^l\},\{n_\beta^l\},\{n_\gamma^l\}\rangle = 1/\left[\sum_{l_2}\sum_{l_1}\left(\frac{dn_{\gamma(\alpha+\beta)}^{l_1+l_2}}{dt}\right)+\sum_{l_2}\sum_{l_1}\left(\frac{dn_{\alpha(\alpha+\gamma)}^{l_1+l_2}}{dt}\right)+\sum_{l_2}\sum_{l_1}\left(\frac{dn_{\beta(\beta+\gamma)}^{l_1+l_2}}{dt}\right)+\sum_{l_2}\sum_{l_1}\left(\frac{dn_{\gamma(\gamma+\gamma)}^{l_1+l_2}}{dt}\right)\right]\cdot\frac{1}{V}$$

$$= 1/\left[\sum_{l_2}\sum_{l_1}k_{\alpha\beta}n_\alpha^{l_1}n_\beta^{l_2}+\sum_{l_2}\sum_{l_1}k_{\alpha\gamma}n_\alpha^{l_1}n_\gamma^{l_2}+\sum_{l_2}\sum_{l_1}k_{\beta\gamma}n_\beta^{l_1}n_\gamma^{l_2}+\sum_{l_2}\sum_{l_1}k_{\gamma\gamma}n_\gamma^{l_1}n_\gamma^{l_2}\right]\cdot\frac{1}{V} \quad (8)$$

where V represents the volume of the system. Since $k = k_{\alpha\beta} = 2k_{\alpha\gamma} = 2k_{\beta\gamma} = 2k_{\gamma\gamma}$, and the particle density $n = N/V$, we obtain

$$\Delta t\langle\{n_\alpha^l\},\{n_\beta^l\},\{n_\gamma^l\}\rangle = 1/\left[\sum_{l_2}\sum_{l_1}n_\alpha^{l_1}n_\beta^{l_2}+\frac{1}{2}\sum_{l_2}\sum_{l_1}n_\alpha^{l_1}n_\gamma^{l_2}+\frac{1}{2}\sum_{l_2}\sum_{l_1}n_\beta^{l_1}n_\gamma^{l_2}+\frac{1}{2}\sum_{l_2}\sum_{l_1}n_\gamma^{l_1}n_\gamma^{l_2}\right]\cdot\frac{1}{kV}$$

$$= 1/\left[\sum_{l_2}\sum_{l_1}N_\alpha^{l_1}N_\beta^{l_2}+\frac{1}{2}\sum_{l_2}\sum_{l_1}N_\alpha^{l_1}N_\gamma^{l_2}+\frac{1}{2}\sum_{l_2}\sum_{l_1}N_\beta^{l_1}N_\gamma^{l_2}+\frac{1}{2}\sum_{l_2}\sum_{l_1}N_\gamma^{l_1}N_\gamma^{l_2}\right]\cdot\frac{V}{k} \quad (9)$$

The time dependence of the chain length distribution and average chain length were obtained by averaging over many simulation runs. The average chain length L_{av} and the reciprocal of the single nanowire fraction $1/f^1$ are given by

$$L_{av} = \frac{\sum_i\sum_l ln^l}{\sum_i\sum_l N_i^l} = \frac{N_0}{\sum_i\sum_l N_i^l} \quad (10)$$

$$1/f^1 = \frac{N_0}{N_\alpha^1 + N_\beta^1} \quad (11)$$

Figure 9a shows average chain length L_{av} vs time obtained for simulations with different initial values of N_0. The results are plotted vs time in units of V/k. The average chain length increases linearly with time and the slope, which corresponds to the rate of assembly, increases as the total number of nanowires increases. By replotting the average chain length vs n_0kt the simulation results collapse onto a universal curve with a slope of one, as shown in Figure 9b.

Figure 10 shows the corresponding plots of the inverse fraction of single (unattached) nanowires $1/f^1$. The rate of assembly of single nanowires is faster than a simple second-order reaction ($1/f^1 \propto$ time) with respect to the single nanowire concentration since a chain formed by attachment of two single nanowires can further react with other nanowires or nanowire chains to form a longer chain.

Directed End-to-End Assembly and Polycondensation. The directed end-to-end assembly of nanowires is conceptually similar to the polycondensation of two monomers, each with two polymerization sites (e.g., A−A and B−B). The kinetics of this type of polycondensation reaction was solved by Flory.[32−34] Assuming that the rate of consumption of the polymerization sites (not the monomers) is second-order we can write

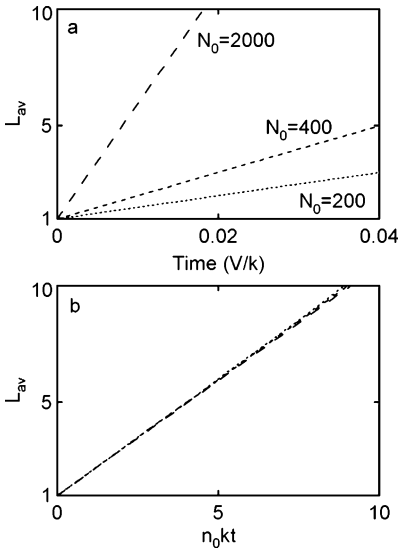

Figure 9. Average chain length vs time obtained from kinetic Monte Carlo simulations of assembly of avidin-terminated nanowires with biotin-terminated nanowires. N_0 is the total number of nanowires in the simulations.

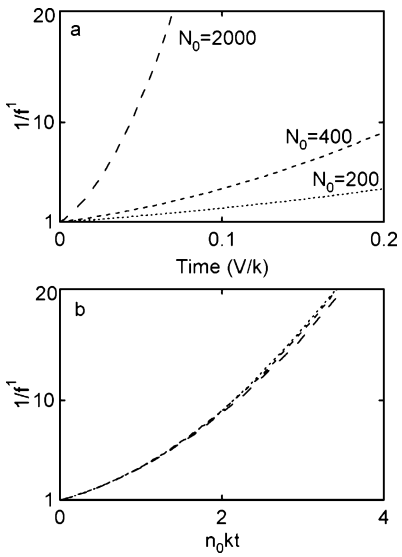

Figure 10. Reciprocal of the fraction of single (unattached) nanowires obtained from kinetic Monte Carlo simulations of assembly of avidin-terminated nanowires with biotin-terminated nanowires. N_0 is the total number of nanowires in the simulations.

$$\frac{dn_A}{dt} = -kn_An_B \quad (12)$$

where n_A and n_B are the time dependent concentrations of the functional terminals. When the initial monomer concentrations are equal, $n_A = n_B = n$ and hence

$$\frac{dn}{dt} = -kn^2 \quad (13)$$

TABLE 1: Values for the Slope and Intercept L_0 of the Plots of Average Chain Length L_{Av} vs $1/n_0kt$ Obtained at (a) Low Shaking Rate (See Figure 7a) and (b) High Shaking Rate (See Figure 7b)

	n_0 (cm^{-3})	slope (s^{-1})	L_0
a	5×10^6	$(6.53 \pm 2.04) \times 10^{-5}$	1.58 ± 0.06
	5×10^7	$(5.72 \pm 3.51) \times 10^{-4}$	1.58 ± 0.08
	1.25×10^8	$(1.41 \pm 0.16) \times 10^{-3}$	1.52 ± 0.18
b	1.25×10^7	$(1.10 \pm 0.18) \times 10^{-3}$	1.9 ± 0.1
	2.5×10^7	$(2.37 \pm 0.39) \times 10^{-3}$	2.6 ± 0.3

Integration gives

$$\frac{1}{n} - \frac{1}{n_0} = kt \tag{14}$$

where n_0 is the initial concentration of functional groups (A or B). Note that since each monomer has two function groups, n_0 is also equal to the total initial monomer concentration. Recall that in our assembly experiments n_0 is similarly defined as the total number of nanowires initially present. Rearranging, we obtain

$$\frac{n_0}{n} - 1 = n_0kt \tag{15}$$

The number-average of the molecular weight distribution is given by

$$n^l = (1\text{-}p)p^{l-1} \tag{16}$$

where n^l is the number of chains of length l, and p is the extent of reaction defined as the ratio of the number of reacted functional terminals to the total number of functional terminals initially present. The average chain length is given by

$$L_{av} = \sum ln^l = \sum l(1-p)p^{l-1} = \frac{1}{1-p} = \frac{n_0}{n} \tag{17}$$

Combination of eqs 15 and 17 and defining an initial average chain length L_0 gives

$$L_{av} - L_0 = n_0kt \tag{18}$$

For the case where only monomers are present at the start of the reaction, $L_0 = 1$. More generally, as in our experiments where the avidin-terminated nanowires were prepared by injecting biotin-terminated nanowires into a large excess of avidin, $L_0 > 1$. Equation 18 is identical to the results of the KMC simulations of nanowire assembly shown in Figure 9b where $L_{av} \propto n_0kt$.

Comparison of Model and Experiments. From the slopes of the plots of L_{av} vs time in Figure 7, we can extract the values for the rate constants for directed end-to-end assembly. The slopes and intercepts of the linear fits for each experiment are presented in Table 1. Figure 11 shows the experimental results replotted as $L_{av} - L_0$ vs n_0kt for the two sets of experiments at different agitation rates. Figure 11a shows the average chain length from the first series of experiments replotted vs n_0kt using a rate constant $k = 1.2 \times 10^{-11}$ cm^3 s^{-1} and $L_0 = 1.5$. The experimental results collapse onto a universal curve consistent with eq 18. The intercept of $L_0 = 1.5$ is due to the fact that some binding occurs when preparing the avidin terminated nanowires, even though there is a large excess of avidin. These chains are expected to be avidin-terminated (type α) due to the large excess of avidin. The agreement of L_0 in all three experiments also confirms that this deviation is from the distribution of avidin-terminated nanowires.

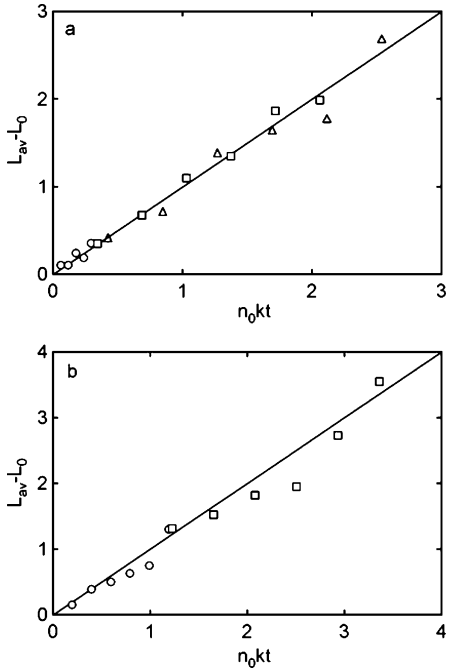

Figure 11. (a) Average nanowire chain length vs n_0kt for three experiments using $k = 1.2 \times 10^{-11}$ cm^3 s^{-1} and $L_0 = 1.5$. $n_0 =$ (○) 5×10^6, (□) 5×10^7, and (△) 1.25×10^8 cm^{-3}. (b) Average nanowire chain length vs n_0kt for two experiments using $k = 9.1 \times 10^{-11}$ cm^3 s^{-1} and $L_0 = 2.3$. $n_0 =$ (○) 1.25×10^7 and (□) 2.5×10^7 cm^{-3}.

Figure 11b shows the results from the second set of experiments with higher agitation rate. The results collapse onto the universal curve with a rate constant $k = 9.1 \times 10^{-11}$ cm^3 s^{-1} and $L_0 = 2.3$. The avidin-terminated nanowires were also prepared at a higher shaking rate, resulting in a slightly larger value of L_0. Because of the fact that this set of experiments were carried out at a much higher shaking rate, the rate constant is about 8 times larger than the experiments shown in Figure 11a.

Figure 12a shows a plot of $1/f^1$ vs time for the three experiments presented in Figure 7a. When the data vs $1/n_0k$ are replotted using the rate constant $k = 1.2 \times 10^{-11}$ cm^3 s^{-1}, the results from the three experimental results collapse onto a universal curve. Since the measurement of single (unattached) nanowires is partially decoupled from the measurement of the average chain length, these results provide further confirmation of the diffusion limited aggregation model.

The time between attachment events increases with time as the nanowire density decreases. We define the collision time τ as the time for the first attachment event. From eq 13, taking $dn = 1/V$ and $dt = \tau$, and recognizing that for the first attachment event $n = n_0$, at constant volume we obtain

$$\tau = \frac{1}{kn_0^2V} = \frac{1}{kn_0N_0} \tag{19}$$

Figure 13 shows the dependence of the collision time on the total number of nanowires in our experiments. In the first set of experiments, the collision time τ decreases from 3.3 ms for a total nanowire density $n_0 = 5 \times 10^6$ cm^{-3} to 5.3 μs at a density $n_0 = 1.25 \times 10^8$ cm^{-3} where $V = 1$ mL. In the second set of experiments, the collision times are 17 and 70 μs at densities n_0 of 2.5×10^7 and 1.25×10^7 cm^{-3}, respectively. As expected,

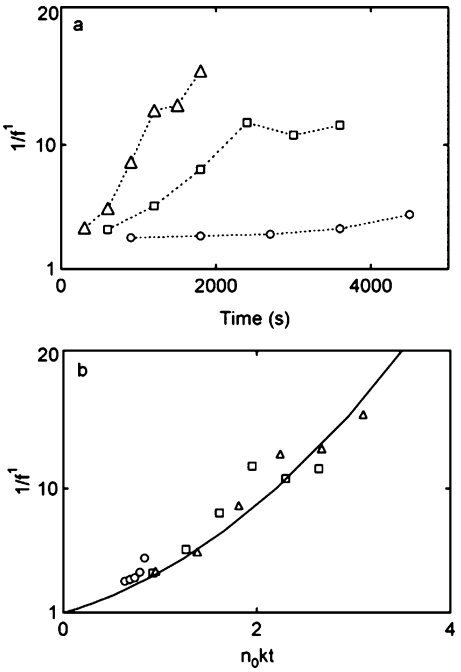

Figure 12. (a) Reciprocal of the fraction of single (unattached) nanowires ($1/f^1$) vs time for experiments with $n_0 = (\bigcirc)\ 5 \times 10^6$, ($\square$) 5×10^7, and ($\triangle$) 1.25×10^8 cm^{-3}. (b) Experimental results replotted vs $1/n_0k$ using $k = 1.2 \times 10^{-11}$ cm^3 s^{-1}.

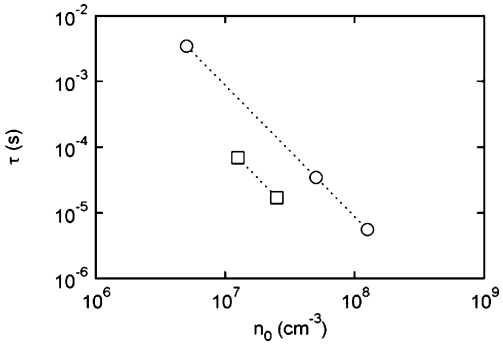

Figure 13. Collision time τ vs initial nanowire concentration from the two sets of experiments shown in Figures 7 and 11.

the rate constant and collision time are both dependent on shaking rate.

Although the nanowires are more than 3 orders of magnitude larger than typical molecular monomers, the analysis of dynamics results illustrate that the end-to-end assembly of nanowires can be described by the collision model derived for step polymerization.

Conclusions

We have demonstrated receptor-directed end-to-end assembly of multisegment Au/Ni/Au nanowires. The incorporation of short gold end-segments with an aspect ratio of about 0.03 minimizes the probability of overlap or the formation of nodes with more than two nanowires. This approach to self-assembly can be extended by incorporating single or multiple linker segments along the length of a nanowire. Various architectures can be constructed on substrates using patterned surfaces to tether nanowires to the surface.

The kinetics of the assembly process can be described by a diffusion-limited aggregation process analogous to linear polycondensation where the average chain length increases linearly with time and is dependent on the nanowire density and convection. These results provide a framework for the design of experiments to produce nanowire chains of specific lengths.

Acknowledgment. This work was supported by the David and Lucile Packard Foundation (Grant No. 2001-17715), and the DARPA Biomagnetics Program (DARPA/AFOSR Grant No. F49620-02-1-0307).

References and Notes

(1) Puntes, V. F.; Krishnan, K. M.; Alivisatos, A. P. *Science* **2001**, *291*, 2115−2117.
(2) Zeng, H.; Li, J.; Liu, J. P.; Wang, Z. L.; Sun, S. H. *Nature* **2002**, *420*, 395−398.
(3) Velev, O. D.; Jede, T. A.; Lobo, R. F.; Lenhoff, A. M. *Nature* **1997**, *389*, 447−448.
(4) Wijnhoven, J. E. G. J.; Vos, W. L. *Science* **1998**, *281*, 802−804.
(5) Jiang, P.; Hwang, K. S.; Mittleman, D. M.; Bertone, J. F.; Colvin, V. L. *J. Am. Chem. Soc.* **1999**, *121*, 11630−11637.
(6) Bezryadin, A.; Westervelt, R. M.; Tinkham, M. *Appl. Phys. Lett.* **1999**, *74*, 2699−2701.
(7) Hayward, R. C.; Saville, D. A.; Aksay, I. A. *Nature* **2000**, *404*, 56−59.
(8) Giersig, M.; Mulvaney, P. *J. Phys. Chem.* **1993**, *97*, 6334−6336.
(9) Taton, T. A.; Mirkin, C. A.; Letsinger, R. L. *Science* **2000**, *289*, 1757−1760.
(10) Aslan, K.; Luhrs, C. C.; Perez-Luna, V. H. *J. Phys. Chem. B* **2004**, *108*, 15631−15639.
(11) Connolly, S.; Cobbe, S.; Fitzmaurice, D. *J. Phys. Chem. B* **2001**, *105*, 2222−2226.
(12) Caswell, K. K.; Wilson, J. N.; Bunz, U. H. F.; Murphy, C. J. *J. Am. Chem. Soc.* **2003**, *125*, 13914−13915.
(13) von Schulthess, G. K.; Benedek, G. B.; de Blois, R. W. *Macromolecules* **1983**, *16*, 434−440.
(14) Lynch, N. J.; Kilpatrick, P. K.; Carbonell, R. G. *Biotechnol. Bioeng.* **1996**, *50*, 151−168.
(15) Kisak, E. T.; Kennedy, M. T.; Trommeshauser, D.; Zasadzinski, J. A. *Langmuir* **2000**, *16*, 2825−2831.
(16) Tresback, J. S.; Vasiliev, A. L.; Padture, N. P. *J. Mater. Res.* **2005**, *20*, 2613−2617.
(17) Martin, B. R.; Dermody, D. J.; Reiss, B. D.; Fang, M. M.; Lyon, L. A.; Natan, M. J.; Mallouk, T. E. *Adv. Mater.* **1999**, *11*, 1021−1025.
(18) Kovtyukhova, N. I.; Mallouk, T. E. *Chemistry* **2002**, *8*, 4355−4363.
(19) Kovtyukhova, N. I.; Martin, B. R.; Mbindyo, J. K. N.; Smith, P. A.; Razavi, B.; Mayer, T. S.; Mallouk, T. E. *J. Phys. Chem. B* **2001**, *105*, 8762−8769.
(20) Piraux, L.; George, J. M.; Despres, J. F.; Leroy, C.; Ferain, E.; Legras, R.; Ounadjela, K.; Fert, A. *Appl. Phys. Lett.* **1994**, *65*, 2484−2486.
(21) Liu, K.; Nagodawithana, K.; Searson, P. C.; Chien, C. L. *Phys. Rev. B* **1995**, *51*, 7381−7384.
(22) Ji, C. X.; Oskam, G.; Ding, Y.; Erlebacher, J. D.; Wagner, A. J.; Searson, P. C. *J. Electrochem. Soc.* **2003**, *150*, C523−C528.
(23) Nicewarner-Pena, S. R.; Freeman, R. G.; Reiss, B. D.; He, L.; Pena, D. J.; Walton, I. D.; Cromer, R.; Keating, C. D.; Natan, M. J. *Science* **2001**, *294*, 137−141.
(24) Wu, Y.; Xiang, J.; Yang, C.; Lu, W.; Lieber, C. M. *Nature* **2004**, *430*, 61−65.
(25) Li, D. Y.; Wu, Y.; Fan, R.; Yang, P. D.; Majumdar, A. *Appl. Phys. Lett.* **2003**, *83*, 3186−3188.
(26) Mokari, T.; Rothenberg, E.; Popov, I.; Costi, R.; Banin, U. *Science* **2004**, *304*, 1787−1790.
(27) Salem, A. K.; Searson, P. C.; Leong, K. W. *Nat. Mater.* **2003**, *2*, 668−671.
(28) Salem, A. K.; Chen, M.; Hayden, J.; Leong, K. W.; Searson, P. C. *Nano Letters* **2004**, *4*, 1163−1165.
(29) Salem, A. K.; Chao, J.; Leong, K. W.; Searson, P. C. *Adv. Mater.* **2004**, *16*, 268−271.
(30) Roe, S. Separation based on structure. In *Protein purification methods: a practical approach*; Harris, E. L. V., Angal, S., Eds.; IRL Press: Oxford, U.K., 1989.
(31) Smoluchowski, M. Z. *Phys. Chem.* **1917**, *92*, 129−168.
(32) Flory, P. J. *J. Am. Chem. Soc.* **1936**, *58*, 1877−1885.
(33) Flory, P. J. *J. Am. Chem. Soc.* **1939**, *61*, 3334−3340.
(34) Flory, P. J. *J. Am. Chem. Soc.* **1942**, *64*, 2205−2212.